Journal of Molecular Liquids 314 (2020) 113645

Contents lists available at ScienceDirect

Journal of Molecular Liquids

journal homepage: www.elsevier.com/locate/molliq

Stability and structural aspects of complexes forming between aluminum (III) and D-heptagluconate in acidic to strongly alkaline media: An unexpected diversity

Ákos Buckó [a], Bence Kutus [b,*], Gábor Peintler [a], Zoltán Kele [c], István Pálinkó [a], Pál Sipos [a,*]

[a] Material and Solution Structure Research Group, Institute of Chemistry, University of Szeged, H–6720 Szeged, Dóm tér 7, Hungary
[b] Department of Molecular Spectroscopy, Max Planck Institute for Polymer Research, 55128 Mainz, Ackermannweg 10, Germany
[c] Department of Medical Chemistry,University of Szeged, H–6720 Szeged, Dóm tér 8, Hungary

ARTICLE INFO

Article history:
Received 28 March 2020
Received in revised form 16 June 2020
Accepted 18 June 2020
Available online 20 June 2020

Keywords:
Aluminate
D–heptagluconate
Formation constants
Speciation
Potentiometry
Polarimetry
NMR
ESI–MS

ABSTRACT

In the current contribution, the complex formation equilibria between Al^{3+} and α-D–heptagluconate ($Hpgl^-$) ions, which is of relevance in, *e.g.,* the Bayer process for obtaining alumina from bauxitic ores, has been investigated. Potentiometric titrations and polarimetric measurements performed at 25 °C and 4 M ionic strength uncovered the formation of several complexes forming in the hyperalkaline (pH ≥ 13) pH range: $Al(OH)_4Hpgl^{2-}$, $Al(OH)_5Hpgl^{3-}$, $Al(OH)_5Hpgl_2^{4-}$, $Al_3(OH)_{13}Hpgl_2^{6-}$ and $Al_4(OH)_{15}Hpgl_3^{6-}$. NMR spectroscopy measurements revealed that diverse complexation processes took place in the hyperalkaline region. In the 9 to 7 pH range, ligand–stabilized aluminum hydroxides were formed. In acidic medium, the binding sites of the ligand could be identified as C2H(OH), C3H(OH), C4H(OH) and C5H(OH). Freezing point depression (FPD) measurements indicated, that association occurred to a large extent. ESI–MS measurements confirmed the predominant formation of $Al_2(OH)_6Hpgl^-$ at pH = 7, and implied the coordination *via* the carboxylate and the adjacent OH functional groups of the ligand.

1. Introduction

Aluminum is the most abundant metal in the earth's crust, which by mass makes up 8% of earth's solid surface. It is an important constituent of many volcanic rocks, feldspars and micas; however, its most important mineral in economic terms is bauxite [1]. Its high aluminum content and the relative ease with which it can be mined, makes bauxite the most important source for aluminum production. The demand for metallurgical grade aluminum gradually increases, and the global annual consumption of bauxite exceeded 200 million tons in 2007 [2].

Almost 97% of the bauxite mined is used to produce alumina (Al_2O_3) *via* the Bayer process. Most bauxite deposits contain various amounts of organic compounds, such as alditols, carboxylates, oils and fatty acids. These substances can enter the Bayer process in various ways: as products of partial decomposition of organic matter in bauxite, as chemical additives, such as flocculants and water treatment reagents, as well as from process machinery by the leakage of lubricant oils. Conversely, their accumulation in the process liquor may have unfavorable impacts on the efficiency of the alumina production. The alleviation of these effects requires complex instrumentation for regulating the amount of organic matter in the process liquor, giving rise to an increase in the production costs [3,4].

Nowadays, lime ($Ca(OH)_2$) is employed on a large scale in the recausticization of the spent liquor to recover NaOH from Na_2CO_3 [2,5]. Similarly to the preceding Bayer process, the presence of organic compounds can affect the conversion of lime recovery either by forming binary Al(III) complexes or by constituting ternary Ca(II)/Al(III) solution species.

As a starting point to understand how organic compounds affect these processes, it is indispensable to gain a deep understanding of the equilibria occurring between Al(III) and organic substances under hyperalkaline conditions (pH ≥ 13). Even though there are some initiative to elucidate the equilibrium properties of these systems [6], the related literature on them is sporadic.

Al^{3+}, being a hard metal ion in the Pearson sense, prefers coordination to hard bases, such as hydroxides, alkoxides and carboxylates. D-gluconate ($Gluc^-$, Scheme 1), being a cheap and prominent member of the hydroxycarboxylates, is widely applied as a model compound for investigating the interactions between organics and various metal ions. In terms of binding strength, $Gluc^-$ benefits from the coexistence of two different functional groups: the COO^- anchor establishes strong binding, which is subsequently increased by

* Corresponding authors.
E-mail addresses: kutusb@mpip-mainz.mpg.de (B. Kutus), sipos@chem.u-szeged.hu,
URL: http://www.staff.u-szeged.hu/~sipos (P. Sipos).

https://doi.org/10.1016/j.molliq.2020.113645

the OH groups in close proximity, leading to the formation of stable chelate complexes. Additionally, deprotonation of at least one OH group at high pH [7,8] yields an alcoholate group. Since it is even stronger base than COO^-, it gives rise to a further enhancement in the complex stability.

The complex equilibria of the Al(III)/$Gluc^-$ system was extensively studied in the pH range of 2–13, revealing the formation of $AlGluc^{2+}$, $Al(OH)Gluc^+$, $Al(OH)_2Gluc^0$, $Al(OH)_3Gluc^-$ [9–12], $Al(OH)Gluc_2^0$ and $Al(OH)_2Gluc_2^-$ [12] as well as $Al(OH)_4Gluc^{2-}$ [13].

As for the structure of the species formed, the OH groups have indeed a unique role: they take part in the metal binding already in acidic solutions, resulting in the formation of stable chelates. The deprotonation of the complexes takes place on the OH groups of the ligand as low as pH ≈ 3, since Al^{3+} is a strong competitor to H^+ for the alcoholate group forming. Based on the results of nuclear magnetic resonance (NMR) experiments, $Gluc^-$ acts as a bi- or tridentate ligand being the C2(OH), C3(OH) and C4(OH) moieties are the most probable binding sites in addition to the COO^- ion [8]. During the formation of the $Al(OH)_3Gluc^-$ species, the third proton is assumed to be displaced from one of the water molecules coordinated to Al^{3+}.

Later, Pallagi et al. reported the predominant existence of the $Al(OH)_4Gluc^-$ species in strongly alkaline medium [13]. Instead of ligand deprotonation, the formation takes place *via* a pH-independent condensation reaction of $Al(OH)_4^-$ ion with two alcoholic OH groups, resulting in a tetrahedral symmetry around Al^{3+}. Furthermore, the COO^- group is not involved in the binding of the metal ion. Thus, the structure of this species is markedly different from those forming below pH ≈ 10,

In conclusion, association reactions between Al^{3+} and hydroxycarboxylates are expected to yield stable mononuclear complexes where metal ion-binding takes place *via* the COO^- and the (deprotonated) OH groups in acidic to mildly basic medium, while condensation reactions start to dominate at high pH (> 11).

Motivated by these results, we embarked on studying the complex formation between Al^{3+} and D-heptagluconate ions ($Hpgl^-$, Fig. 1), being the latter a close analogue of $Gluc^-$. Different from the previous studies, however, we employed a broad range of pH (2–14), metal and ligand concentrations in order to gain a comprehensive picture on the equilibrium and structural aspects of such a complicated system. To achieve this goal, we applied potentiometry, polarimetry, freezing point depression, NMR spectroscopy as well as electrospray ionization mass spectrometry (ESI-MS). Additionally, we discuss the effect of heptagluconate ions on the solubility of gibbsite.

2. Materials and methods

2.1. Reagents and solutions

All solutions were prepared by using deionized water (Merck Millipore Milli-Q®) and the ionic strength was adjusted with NaCl (VWR, a. r. grade). Sodium α-D-heptagluconate (Sigma-Aldrich, ≥99% purity) was purchased as hydrated salt. The water content was determined by weighing the solid before and after heating it at 80 °C for six hours. Additionally, the purity of $Hpgl^-$ sodium salt was attested by recording its ^1H and ^{13}C NMR spectra. No signals of contaminants were found which peak area was greater than 1% compared to the total peak area of the ligand.

1 M NaOH stock solutions were made of 50 *w*/w% carbonate-free NaOH solution which was prepared from NaOH pellets (VWR, a. r. grade) according to the procedure reported in Ref. [14]. The required amount of *cc.* NaOH was diluted to 1 dm^3 volume and standardized against HCl solution. The stock solutions of acid were made by volumetric dilution of approx. 37 w/w% HCl (a.r. grade, Scharlau) and were standardized with $KHCO_3$ solution. Sodium aluminate solutions (≈ 4 M $NaAl(OH)_4$, ≈ 4 M excess NaOH) were prepared according to procedures described earlier [15], *i.e.*, by dissolving aluminum wires (J.M. & Co., 99.99% purity) in the carbonate-free NaOH solution. The concentration of $Al(OH)_4^-$ was determined by two methods. First, the metal as well as the filtered stock solution after the dissolution reaction was weighed. To convert the mass to volume, the density of the final solution was determined by a 25 mL pycnometer at (25.0 ± 0.1) °C. Second, a ≈ 0.02 M $NaAl(OH)_4$ solution was prepared from the concentrated one and the metal content was determined *via* an EDTA titration at pH ≈ 2. The agreement between the values obtained from the two methods was within 1%.

2.2. Potentiometry

Potentiometric titrations were performed using a titroprocessor (Metrohm 888 Titrando using tiamo™ 2.5 software for titration control, Metrohm AG, Switzerland) employing a SenTix®-62 (from WTW) combined glass (GLE) or a platinized platinum electrode (H_2/Pt); the latter was prepared according to Ref. [16]. The electrochemical cell consisted of the indicator (GLE or H_2/Pt) and an Ag/AgCl reference electrode. The measurements were executed in a closed custom-made titration vessel, covered with a PTFE lid and externally thermostated to (25.0 ± 0.1) °C with a Julabo F12-MB thermostat.

The GLE and H_2/Pt electrodes were calibrated by titrating a weak acid (0.070 M malonic acid, Fluka, a. r. grade) and a strong acid (0.150 M HCl) with ≈1 M NaOH solutions by the protocol described in detail in the manual of the pHCali software [17]. During the fitting procedure, the log K_w was fixed to −14.26 [8]. As a result of the calibration, the H_2/Pt and GLE electrodes were found to be Nernstian in the range of $1.9 < pH_c < 13.6$ and $1.9 < pH_c < 10.9$, respectively (where pH_c is defined as $-\log([H^+]/c^\ominus)$).

To study the protonation of $Hpgl^-$, two sets of solutions with $[Hpgl^-]_{T,0} = 0.050$ M and 0.200 M were titrated with a 1.0056 M HCl solution, using GLE (in all other cases, H_2/Pt was applied). Hereafter for component X, the analytical concentration is denoted as $[X]_{T,0}$ (at the starting point of a titration) or $[X]_T$ (polarimetric, NMR and freezing point depression experiments), while [X] is referred to as the equilibrium concentration.

During the deprotonation measurements, $[Hpgl^-]_{T,0}$ was varied between 0.100 and 0.400 M, while $[NaOH]_{T,0}$ was 0.005 M. The titrant was 1.0114 M NaOH. To investigate the complexation of Al(III), $[Al(OH)_4^-]_{T,0}$, $[Hpgl^-]_{T,0}$ and $[NaOH]_{T,0}$ were varied in the range of 0.100–0.400 M, 0.176–0.400 M and 0.051–0.204 M, respectively. The titrant was 0.9889 M HCl with the ionic strength (*I*) set to 5 M to avoid the decrease in background electrolyte concentration caused by neutralization. In all other cases, *I* was adjusted to 4 M. For each

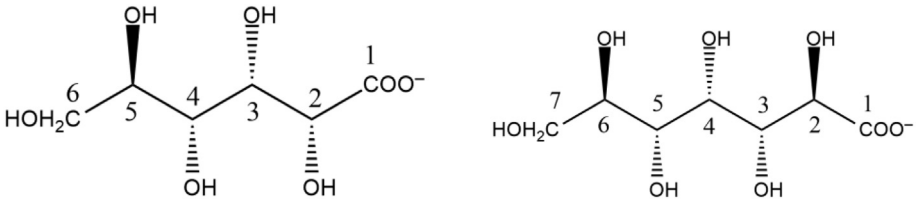

Fig. 1. Structural formulas of D-gluconate (left) and D-heptagluconate (right).

titration, the starting and final volumes (V) were 70 and 120 mL, respectively, except for the one solution with $[NaOH]_{T,0} = 0.401$ M, where the titration ended at $V = 140$ mL.

Due to the rather slow kinetics known for Al(III) in acidic medium, the titrations were performed by setting different minimum and maximum waiting times to check if the "equilibrium" cell potentials show time-dependence. The observed potential was accepted if the signal drift did not exceed the maximum tolerance interval (± 0.3 mV) after the minimum waiting time. We found that in order to attain chemical equilibrium in the entire pH range, the minimum waiting time must be 20 min (while the maximum was set to 40 min).

2.3. Polarimetry

Optical rotation measured using a Lippich-type polarimeter (Krüss P-1000, A.KRÜSS Optronic GmbH, Hamburg, Germany) equipped with LED light source. The degrees of rotation (θ) were measured on the wavelength of the sodium D line (589 nm) using polarimeter tubes with 200 mm path length at room temperature (23 ± 2) °C. The reading accuracy of the instrument was ±0.05°.

In order to follow the complex formation and to calculate the molar rotation of the individual species ($[\Phi]$), the following solutions were prepared: at constant $[OH^-]_T$ (0.200 M), $[Hpgl^-]_T$ was set to 0.100, 0.200 and 0.400 M, respectively, while $[Al(OH)_4^-]_T$ was gradually increased up to 0.800 M. A NaOH-dependent series contained 0.175 M NaHpgl, 0.200 M $NaAl(OH)_4$ with $[OH^-]_T$ varying from 0.025 to 0.500 M. In each case, I was set to 4 M.

2.4. Nuclear magnetic resonance (NMR)

^1H and ^{13}C NMR spectra were recorded with a Bruker Avance III HD 500 MHz NMR spectrometer equipped with a 5 mm inverse broadband probe head (CryoProbe™ Prodigy) furnished with z-oriented magnetic-field-gradient capability. The magnetic field was stabilized by locking it to the ^2D signal of the solvent prior to spectral acquisition. No solvent suppression was used and the baseline was numerically subtracted from each spectra. The temperature was maintained at (25 ± 1) °C and 10% (V/V) D_2O was added to each sample. The assignment of the ^1H peaks of $Hpgl^-$ was based on literature [18], while that of the ^{13}C nuclei was performed by a ^1H—^{13}C heteronuclear single quantum correlation spectrum for a 0.5 M NaHpgl solution (Fig. S1).

To study the effect of metal ion and pH on the spectra of the ligand, two sets of solutions were prepared. First, $[Al(OH)_4^-]_T$ was varied between 0 and 0.800 M with $[Hpgl^-]_T$ being 0.200 M, while the pH was set to 4, 8 and 12. Second, the pH was gradually increased by one unit from 4 to 12 with $[Hpgl^-]_T$ and $[Al(OH)_4^-]_T$ being 0.200 M. The pH values of the solutions were set using GLE, which was calibrated with dilute buffers. Due to the different activity coefficient of H^+ in the buffers from that in the samples, the pH adjusted here is regarded as nominal, directly recorded from the pH meter. To minimize the differences between pH and pH_c, background electrolyte was not added to the samples.

128 and 1024 interferograms were collected to obtain the ^1H and ^{13}C NMR spectra, excluding pH = 4 and 12, where in case of the ^{13}C NMR spectra 8096 scans were applied instead. For comparison, the spectra were baseline-corrected and normalized.

2.5. Freezing point depression (FPD)

Freezing point depression was measured with a Testo 735 digital precision thermometer using a probe with an accuracy of ±0.05 °C. The change of temperature was monitored and recorded in every second during the measurements. The coolant was a mixture of water, ice and $MgCl_2 \cdot 6H_2O$. One set of samples were prepared by varying $[Al(OH)_4^-]_T$ from 0.100 to 0.800 M (at $[Hpgl^-]_T = 0.200$ M). Additional experiments were conducted using $[Al(OH)_4^-]_T = 0.200$ M (varying $[Hpgl^-]_T = 0.100$–0.400 M) as well as with $[OH^-]_T$ ranging from 0.050 to 0.500 M.

2.6. Electrospray ionization mass spectrometry (ESI–MS)

The mass spectra of solutions containing $[Hpgl^-]_T = [Al(OH)_4^-]_T = 0.001$ M at $pH_{nom} = 7$ and 12 were recorded in negative mode using a Micromass Q-TOF Premier (Waters MS Technologies, Manchester, UK) mass spectrometer equipped with an electrospray ion source. The samples were introduced into the MS by applying direct injection method: the built-in syringe pump of the instrument with a 25 mL Hamilton syringe was used. The electrospray needle was adjusted to 3 kV and N_2 was used as nebulizer gas. The computer program used to simulate the theoretical isotope distributions is included in the Masslynx software [19].

2.7. Data evaluation and speciation calculations

The general complexation reaction between $Al(OH)_4^-$ and $Hpgl^-$ ions as well as the corresponding stability product, β_{pqr}, read as:

$$pAl(OH)_4^- + qHpgl^- + rH^+ \rightleftharpoons Al_p(OH)_{4p-r}Hpgl_q^{(p+q-r)-} + rH_2O \quad (1)$$

$$\beta_{pqr} = \frac{\left[Al_p(OH)_{4p-r}Hpgl_q^{(p+q-r)-}\right]^p}{\left[Al(OH)_4^-\right]} [Hpgl^-]^q [H^+]^r \left(c^{\varnothing}\right)^{1-p-q-r} \quad (2)$$

where $c^{\varnothing}$ is the standard molar concentration of unity, $c^{\varnothing} = 1$ M. The equilibrium constants as well as molar rotations of the species forming were calculated with the aid of the PSEQUAD [20] software. Throughout the fitting procedure, the so-called fitting parameter (FP) was minimized:

$$FP = \sqrt{\frac{\sum_{i=1}^{n} \left(Y_{i,calc} - Y_{i,meas}\right)^2}{n-k}} \quad (3)$$

where $Y_{i,calc}$ and $Y_{i,meas}$ represent the calculated and measured i^{th} data (pH_c or θ), while n refers to the number of measured data and k to the number of fitted parameters. When polarimetric and potentiometric data are fitted together, eq. (3) could be written in the following form:

$$FP = \sqrt{\frac{\sum_{i=1}^{m} w_1 (\Delta E_i)^2 + \sum_{i=m+1}^{n} w_2 (\Delta\theta_i)^2}{n-k}}^{-2} \quad (4)$$

where $\Delta E_i/\Delta\theta_i$ is the difference of the measured and calculated e.m.f/rotation power data, $w_1 (= 1\ mV^{-2})$ and $w_2 (= 100\ deg.^{-2})$ are the weighting factors for the i^{th} POT or POL dataset of measurements, n refers to the number of measured data and k to the number of fitted parameters and the calculated FP value is a dimensionless number. In case of fitting only one type of data, *e.g.*, potentiometric titration, FP could be read as the error sum square of e.m.f in mV units; in this case $w_1 = 1$.

The speciation calculations were performed by applying the MEDUSA [21] software by setting $Al(OH)_4^-$ as the primary Al(III)-containing species, therefore, $[Al(III)]_T = [Al(OH)_4^-]_T$.

3. Results and discussion

3.1. Complexation between $Al(OH)_4^-$ and $Hpgl^-$ ions

3.1.1. The protonation and deprotonation of $Hpgl^-$. Similarly to other hydroxycarboxylates, it is known that the COO^- group of $Hpgl^-$ undergoes protonation yielding heptagluconic acid (HpglH) [18,23]:

Please cite this article as: Á. Buckó, B. Kutus, G. Peintler, et al., Stability and structural aspects of complexes forming between aluminum(III) and D-heptagluconate in ..., Journal of Molecular Liquids, https://doi.org/10.1016/j.molliq.2020.113645

$$Hpgl^- + H^+ \rightleftharpoons HpglH \quad (5)$$

$$K_p = \beta_{011} = \frac{[HpglH]\cdot c^{\varnothing}}{[Hpgl^-]}[H^+] \quad (6)$$

where K_p is the protonation constant of the anion. Note that according to Eq. 2, $K_p = \beta_{011}$. Fitting the potentiometric curves (Fig. S2) with log $K_p = 3.64$ results in an excellent agreement between the measured and calculated data (FP = 0.40 mV). Furthermore, it agrees with the one reported in Ref. [22], with due account to the different ionic strength. Conversely, a significantly lower value was obtained *via* ^{1}H NMR spectroscopy [18], which most probably stems from the inappropriate calibration of the glass electrode. Furthermore, we find good agreement with the protonation constant of $Gluc^-$, determined at the same ionic strength [8]. All these constants are listed in Table 1.

In strongly alkaline medium, the OH group(s) of $Hpgl^-$ undergoes deprotonation [18]:

$$Hpgl^- \rightleftharpoons HpglH_{-1}^{2-} + H^+ \quad (7)$$

$$K_a = \beta_{01-1} = \frac{\left[HpglH_{-1}^{2-}\right][H^+]}{[Hpgl^-]\cdot c^{\varnothing}} \quad (8)$$

where K_a is the deprotonation constant of $Hpgl^-$. Assuming one deprotonation step with log K_a being −13.81 is sufficient the titration curves depicted in Fig. S3 (FP = 0.25 mV, *i.e.*, 0.004 pH_c units). This constant agrees well with the one obtained at $I = 1$ M NaCl [18], also with the one for $Gluc^-$, determined at the same ionic strength [23].

3.1.1. Qualitative observations for the $Al(OH)_4^-$/$Hpgl^-$ system

In order to elucidate the interactions of $Hpgl^-$ with $Al(OH)_4^-$, we carried out both potentiometric and polarimetric measurements. Whilst the first method is sensitive to any pH-dependent process, the second one is sensible to the formation of complexes where the structure of the optically active ligand is markedly different from that of the bare anion. Combining these two experimental means, *i.e.*, fitting the titration curves and optical rotations simultaneously, can provide a comprehensive picture about the stabilities and compositions of the complexes formed.

For titrations conducted at $[NaOH]_{T,0} = [Al(OH)_4^-]_{T,0} = 0.2$ M (Fig. 2, black curves), the increase of $[Hpgl^-]_{T,0}$ has a considerable impact on the shape of the curves in the pH_c range of ≈10.0–13.3. This shows that the formation of complexes, for which $q/p \geq 2$, takes place mainly in the alkaline medium. Furthermore, the increase of $[Al(OH)_4^-]_{T,0}$ at constant $[NaOH]_{T,0}$ and $[Hpgl^-]_{T,0}$ (0.2 M, Fig. 2, blue curves) results in strong aluminate-dependence of the curves below pH ≈ 10. This is indicative of the formation of multinuclear species, *i.e.*, species with $p > 1$. Additionally, when $[Al(OH)_4^-]_{T,0}/[Hpgl^-]_{T,0} = 2$ (Fig. 2, curve with blue triangles), the ligand cannot keep Al(III) in the solution phase, leading to the precipitation of $Al(OH)_3$ below $pH_c \approx 11.5$. Most importantly, the titration curves clearly show the presence of several inflection points, indicating the complexes formed undergo stepwise protonation as HCl is added to the samples.

Upon increasing $[Al(OH)_4^-]_{T,0}$ at constant $[Hpgl^-]_T$ (Fig. 3), the optical rotation of the ligand exhibit marked increase, that is, from ≈0.5° to 2.5°, 5.5° and 11.5° at $[Hpgl^-]_T = 0.2$, 0.4 and 0.8 M. The ligand possesses five chiral centers, whose relative spatial arrangement (through the HCCH dihedral angles) determines [Φ] and hence θ through the well-known relationship analogous to the Beer–Lambert law. The marked increment in θ, thus, is a strong indicator that the conformation of $Hpgl^-$ undergoes variation to a large extent as a token of complexation with aluminate. Furthermore, the fact that θ increases steeply and then reaches a maximum value (at least for $[Hpgl^-]_T = 0.1$ and 0.2 M) implies high degree of association. We also discern that the maximum value of θ roughly doubles upon twofold increase of $[Hpgl^-]_T$, signaling that the same species is formed almost quantitatively. As for the NaOH-dependent measurements, it is obvious that at least three complexes are formed with different degree of deprotonation.

3.1.2. Quantitative data analysis

For each fit, we fixed the values of log K_w to −14.26 [8], as well as log K_p and log K_a to those obtained in this work. In the next step, we systematically varied the stoichiometric numbers *p*, *q* and *r*, in order to minimize the FP.

To extract the stoichiometry and the corresponding stability constants of the individual complexes data evaluation was performed, where the pH–, $Hpgl^-$– and $Al(OH)_4^-$ –dependent titrations as well as the protonation and deprotonation experiments of the ligand were fitted simultaneously Fig. 2). Supposing the formation of $Al(OH)_4^-$: $Hpgl^-$ = 1:1 stoichiometry species, *i.e* formation of $Al(OH)_5Hpgl^{3-}$, $Al(OH)_4Hpgl^{2-}$, $Al(OH)_3Hpgl^-$, $Al(OH)Hpgl^+$ and $AlHpgl^{2+}$ as well as $HpglH_{-1}^{2-}$ and HpglH, the fitting parameter, FP, was calculated to be 37.47 mV (or 0.63 pH_c units). Along with the various protonated forms of the 1:1 complex, the hydroxido complexes of aluminum was fitted. According to *Eq.* 2, the formation quotients of $Al(OH)^{2+}$, $Al(OH)_2^+$, $Al(OH)_3^0$, $Al_2(OH)_2^{4+}$, $Al_3(OH)_4^{5+}$ and $Al_{13}O_4(OH)_{24}^{7+}$ were fitted together with the previously included species, however these species did not form in a significant (*i.e* detectable) extent. The second series of titrations (blue curves) consisted of solutions containing $[Hpgl^-]_T$ = 0.200 M and $[Al(OH)_4^-]_T$ 0.100–0.400 M, while the third set (red curves) of measurements were performed at $[Hpgl^-]_T = 0.200$ M and $[Al(OH)_4^-]_T = 0.130$ M with the variation of the initial concentration of sodium hydroxide from 0.050 M to 0.400 M. Upon increasing the metal:ligand ratio there was no significant change in the initial value of E_{cell} and the curvature of the curves was practically identical, however a systematic shift towards lower cellpotential values could be observed. Additionally, the formation of precipitation could be detected when $[Al(OH)_4^-]_T$ exceeded $[Hpgl^-]_T$. The increment of $[NaOH]_T$ yielded lower E_{cell} values with congruent curves.

For further improvement, the inclusion of polynuclear complexes, such as the bis-complexes $Al(OH)_5Hpgl_2^{4-}$ and $Al_2(OH)_6Hpgl^-$, the dimeric species $Al_2(OH)_4Hpgl_2^0$ and $Al_2(OH)_5Hpgl_2^-$ and trinuclear $Al_3(OH)_{10}Hpgl^{2-}$ complexes was indispensable, resulting FP = 4.37 mV (or 0.07 pH_c units).

The corresponding chemical model is in line with the qualitative conclusions drawn in the previous section; the respective species and their formation constants are listed in Table 1. For the fitted molar rotations, see Table S1. The simulated titration curves and optical rotations are depicted in Figs. 2 and 3. For detailed discussion of the measured polarimetric curves, see Section S1 in the ESI.

A speciation diagram with corresponding to $[Al(OH)_4^-]_T = [Hpgl^-]_T$ = 0.2 M is shown in Fig. 4. We observe distinct complexation patterns. First, the formation of $AlHpgl^{2+}$ takes place between pH_c 2 and 4, and undergoes stepwise deprotonation yielding $Al(OH)Hpgl^+$, $Al(OH)_3Hpgl^-$, $Al(OH)_4Hpgl^{2-}$ and $Al(OH)_5Hpgl^{3-}$; the latter can bind a further ligand to form $Al(OH)_5Hpgl_2^{4-}$. We cannot discern the formation of the intermediate $Al(OH)_2Hpgl^0$ species, however, we believe that it readily dimerizes, which manifests in the appearance of $Al_2(OH)_4Hpgl_2^0$ at $pH_c > 3$. This species is further deprotonated yielding $Al_2(OH)_5Hpgl^{2-}$.

Furthermore, the formation of $Al_2(OH)_6Hpgl^-$ and $Al_3(OH)_{10}Hpgl^{2-}$ can be interpreted as the abstraction of one or two aluminate ions by $Al(OH)_2Hpgl^0$. Two other polynuclear species appears above $pH_c \approx 8$, namely, the $Al_4(OH)_{15}Hpgl_3^{6-}$ and $Al_3(OH)_{13}Hpgl_2^{6-}$ ones. The tetranuclear complex may be formed *via* the association of $Al_3(OH)_{10}Hpgl^{2-}$ and $Al(OH)_5Hpgl_2^{4-}$, while the appearance of $Al_3(OH)_{13}Hpgl_2^{6-}$ may be the result of the aggregation of $Al(OH)_4Hpgl^{2-}$, $Al(OH)_5Hpgl^{2-}$ and $Al(OH)_4^-$. Additionally, this trinuclear species is the one that gives rise to the marked increase in the optical rotation under hyperalkaline conditions ($pH_c \geq 13$); see the speciation diagrams in Figs. S4–S6. We

Table 1
Stability constants, log β_{pq-r}, determined for the various reactions taking place in the $Al(OH)_4^-$ / $Hpgl^-$ system. Experimental conditions: $T = 25$ °C, $I = 4$ M (NaCl). In parentheses, the triple standard error is given. For analogous gluconate complexes, literature data are also provided.

Reaction	log β_{pq-r}	Method[a]	Ref[b]
$H_2O \rightleftharpoons H^+ + OH^-$	−14.26[c]	H_2/Pt	[8]
	3.64(1)	GLE / POL	p. w.
$Hpgl^- + H^+ \rightleftharpoons HpglH + H_2O$	3.38(2)[c]	GLE	[22]
	2.49(2)[c]	GLE / ^{1}H NMR	[18]
$Gluc^- + H^+ \rightleftharpoons HpglH + H_2O$	3.73(5)[c]	GLE	[23]
$Hpgl^- \rightleftharpoons HpglH_{-1}^{2-} + H^+$	−13.81(1)	H_2/Pt / POL	p. w.
	−13.41(2)[c]	H_2/Pt / POL	[18]
$Gluc^- \rightleftharpoons GlucH_{-1}^{2-} + H^+$	−14.08(3)[c]	H_2/Pt	[8]
	−13.90(3)[c]	^{13}C NMR	[8]
	22.81(19)		p. w.
$Al(OH)_4^- + 4H^+ \rightleftharpoons Al^{3+} + 4H_2O$	23.23[d]	H_2/Pt / POL	[24]
	23.40[e]		[12]
$Al(OH)_4^- + Hpgl^- + 4H^+ \rightleftharpoons AlHpgl^{2+} + 4H_2O$	24.85(29)	H_2/Pt / POL	p. w.
	25.21[c,d]	GLE	[9]
$Al(OH)_4^- + Gluc^- + 4H^+ \rightleftharpoons AlGluc^{2+} + 4H_2O$	25.24(6)[c,d]	GLE	[10]
	25.78(3)[c,e]	GLE	[12]
$Al(OH)_4^- + Hpgl^- + 3H^+ \rightleftharpoons Al(OH)Hpgl^+ + 3H_2O$	22.06(13)	H_2/Pt / POL	p. w.
	22.34[c,d]	GLE	[9]
$Al(OH)_4^- + Gluc^- + 3H^+ \rightleftharpoons Al(OH)Gluc^+ + 3H_2O$	22.35(12)[c,d]	GLE	[10]
	22.39(6)[c,d]	GLE	[11]
	21.91(6)[c,e]	GLE	[12]
$Al(OH)_4^- + Hpgl^- + H^+ \rightleftharpoons Al(OH)_3Hpgl^- + H_2O$	12.28(26)	H_2/Pt / POL	p. w.
	13.05[c,d]	GLE	[9]
$Al(OH)_4^- + Gluc^- + H^+ \rightleftharpoons Al(OH)_3Gluc^- + H_2O$	13.05(24)[c,d]	GLE	[10]
	12.52(6)[c,d]	GLE	[11]
	11.41(3)[c,e]	GLE	[12]
$Al(OH)_4^- + Hpgl^- \rightleftharpoons Al(OH)_4Hpgl^{2-}$	1.89(17)	H_2/Pt / POL	p. w.
$Al(OH)_4^- + Gluc^- \rightleftharpoons Al(OH)_4Gluc^{2-}$	2.4(1.2)[c]	^{1}H NMR	[13]
	2.2(0.6)[c]	POL	[13]
$Al(OH)_4^- + Hpgl^- + H_2O \rightleftharpoons Al(OH)_5Hpgl^{3-} + H^+$	−11.59(29)	H_2/Pt / POL	p. w.
$Al(OH)_4^- + 2Hpgl^- + H_2O \rightleftharpoons Al(OH)_5Hpgl_2^{4-} + H^+$	−9.02(15)	H_2/Pt / POL	p. w.
$2Al(OH)_4^- + Hpgl^- + 2H^+ \rightleftharpoons Al_2(OH)_6Hpgl^- + 2H_2O$	24.98(21)	H_2/Pt / POL	p. w.
$2Al(OH)_4^- + 2Hpgl^- + 4H^+ \rightleftharpoons Al_2(OH)_4Hpgl_2^0 + 4H_2O$	37.99(21)	H_2/Pt / POL	p. w.
$2Al(OH)_4^- + 2Hpgl^- + 3H^+ \rightleftharpoons Al_2(OH)_5Hpgl_2^- + 3H_2O$	33.41(20)	H_2/Pt / POL	p. w.
$3Al(OH)_4^- + Hpgl^- + 2H^+ \rightleftharpoons Al_3(OH)_{10}Hpgl^{2-} + 2H_2O$	28.23(26)	H_2/Pt / POL	p. w.
$3Al(OH)_4^- + 2Hpgl^- + H_2O \rightleftharpoons Al_3(OH)_{13}Hpgl_2^{6-} + H^+$	−6.52(26)	H_2/Pt / POL	p. w.
$4Al(OH)_4^- + 3Hpgl^- + H^+ \rightleftharpoons Al_4(OH)_{15}Hpgl_3^{6-} + H_2O$	21.74(39)	H_2/Pt / POL	p. w.

[a] H_2/Pt, GLE: potentiometry applying a platinum H_2 or glass electrode, POL: polarimetry, NMR: nuclear (^{1}H or ^{13}C) magnetic resonance spectroscopy.
[b] In the present work, the constants were determined *via* the simultaneous fit of potentiometric and polarimetric data.
[c] The stability products correspond to $I = 0.1$ M KNO_3 [9], 0.1 M NaCl [10], 0.1 M $NaNO_3$ [11,23], 0.2 M KCl [12], 1 M NaCl [13,18] and 4 M NaCl [8,24].
[d] The stability products of the analogous gluconate complexes were converted from the literature data [9–11] using the formation constant of $Al(OH)_4^-$ ($I = 0.1$ M) reported in Ref. [24].
[e] The stability products of the analogous gluconate complexes were converted from the literature data [12] using the formation constant of $Al(OH)_4^-$ ($I = 0.2$ M) reported in Ref. [12].

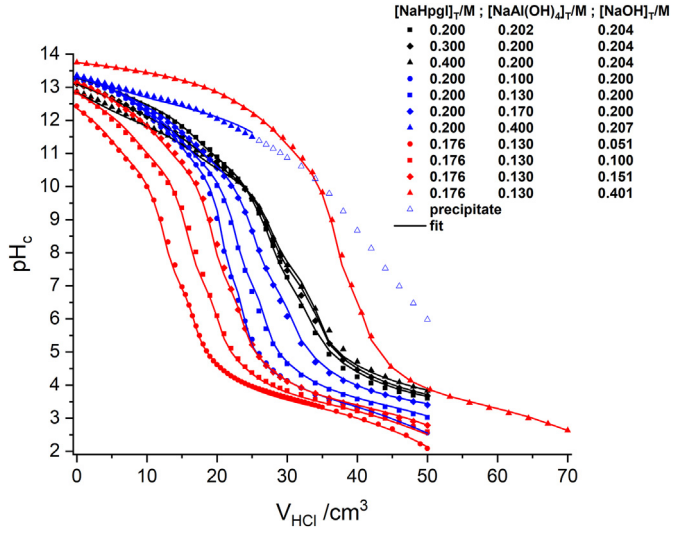

Fig. 2. Measured pHc values (= log ($[H^+]/c^o$) as a function of added titrant volume in solutions consisting of heptagluconate ($Hpgl^-$), $Al(OH)_4^-$ and NaOH. The initial compositions of the samples are shown on the legend. Symbols represent the measured data, lines were fitted on the basis of the speciation model discussed in the text and provided in Table 1. Experimental conditions: $T = (25 \pm 0.1)$ °C and $I = 4$ M (NaCl).

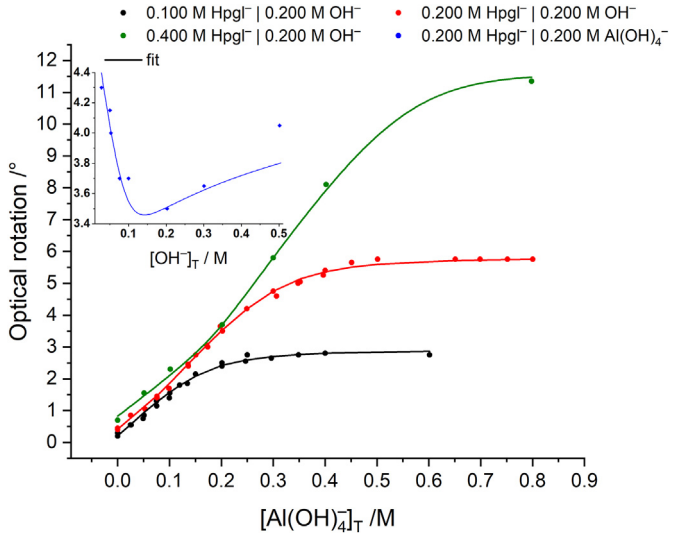

Fig. 3. Optical rotation of D-heptagluconate as a function of added $[Al(OH)^-]_T$ (circle) and pH (diamond). Experimental conditions: T = (25 ± 2)°C and $I = 4$ M (NaCl). Total concentrations: $[Al(OH)_4^-]_T = 0$–0.800 M and $[Hpgl^-]_T = 0.100$–0.400 M. Symbols and lines refer to the measured and calculated values, respectively.

Please cite this article as: Á. Buckó, B. Kutus, G. Peintler, et al., Stability and structural aspects of complexes forming between aluminum(III) and D-heptagluconate in ..., Journal of Molecular Liquids, https://doi.org/10.1016/j.molliq.2020.113645

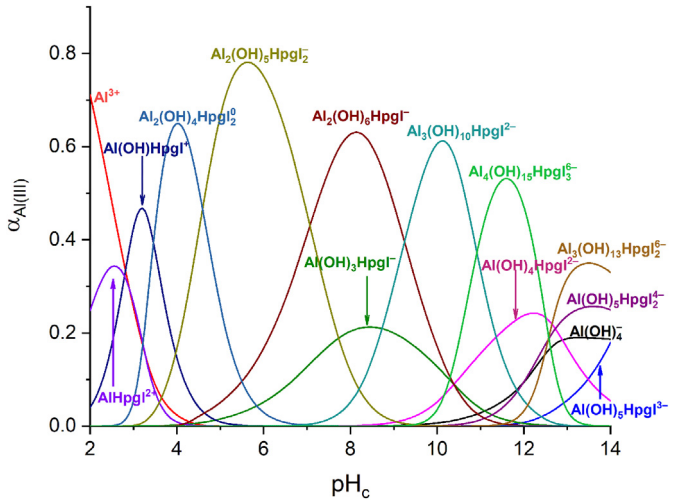

Fig. 4. Speciation diagram as a function of pH_c ($(= \log([H^+]/c^o)$ with regard to Al(III). The calculations were performed using the stability constants provided in Table 1, corresponding to $T = 25$ °C and $I = 4$ M (NaCl). Total concentrations: $[Al(OH)_4^-]_T = [Hpgl^-]_T = 0.200$ M.

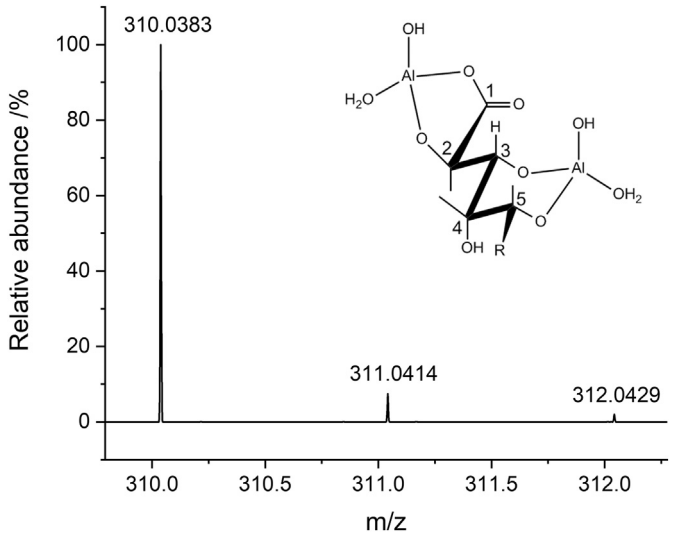

Fig. 5. ESI-MS spectrum of a solution containing $[Al(OH)_4^-]_T = [Hpgl^-]_T = 0.001$ M at pH = 7. The spectrum was recorded in negative ion mode. The peak at 310.0383 *m/z* corresponds to the $Al_2(OH)_6Hpgl^-$ species, predominant in this solution. The inset shows the proposed structure of this species, where 'R' represents the C(6)HOH-C(7)H_2OH moiety and the hydrogens are omitted for clarity.

gain further semi-quantitative validation for the model from the FPD measurements, see Section S2 and Table S2 in the ESI.

Given the complexity of the system and hence the difficulty to pinpoint and properly quantify all individual equilibrium processes, one can question the reliability of the compositions of these complexes. Nevertheless, their inclusion in the model is necessary to give an appropriate proper description for the experimental data and their formation indicates that at high concentrations, simple mononuclear species tend to aggregate.

The plethora of solution species found in this system is rather unexpected, based on previous findings for $Gluc^-$ [9–13], *i.e.*, the exclusive formation of mononuclear species. We would like to emphasize, however, that those previous measurements were conducted in the millimolar concentration range. (Albeit measurements at $pH_c > 12$ were undertaken at $[Al(OH)_4]_{T,0} \approx [Gluc^-]_{T,0} \approx 0.1$ M [13], the authors did not study the concentration-dependence of the titrations curves, which is essential to detect polynuclear complexes.) Indeed, setting $[Al(OH)_4^-]_T$ to 0.002 M and $[Hpgl^-]_T$ to 0.004 M, the complexation equilibria simplifies to that proposed previously (Fig. S7). As for the analogous gluconate complexes, we find that the stability constants are in fair agreement with our data (Table 1); the deviations are ascribable to the much lower ionic strength (0.1–0.2 M) applied in Refs. [9–13]. (Since the primary species was Al^{3+} in Refs. [9–12], we converted them using the formation constant of $Al(OH)_4^-$, taken from Ref. [24].) Based on these similarities between the two ligands, we propose that multinuclear species are likely to be formed with $Gluc^-$ in concentrated solutions, too. This assumption is supported by the fact that the $Ca_3L_2(OH)_4^0$ species dominates the complexation equilibria for both ligands, when $[CaCl_2]_T \approx [L^-]_T \geq 0.05$ M [7,8,23].

3.2. Identification of the $Al_2(OH)_6Hpgl^-$ complex by ESI-MS and its possible structure

We performed ESI–MS measurements in order to gain further experimental support for the chemical proposed in the previous section. The negative ion-mode spectrum shown in Fig. 5 refers to a solution containing $[Al(OH)_4^-]_T = 0.001$ M and $[Hpgl^-]_T = 0.001$ M at pH = 7. To estimate which species is formed under the conditions of the MS experiments, we calculated the speciation using the data in Table 1. Accordingly, $Al_2(OH)_6Hpgl^-$ dominates the pH range 6–8 (the degree of its formation is ≈40% relative to $[Hpgl^-]_T$).

The experimental mass spectrum matches perfectly with a species having a chemical formula of $Al_2C_7H_{12}O_{10}^-$, that is, $Al_2(OH)_2HpglH_{-3}^-$, where $HpglH_{-3}^{4-}$ refers to the threefold deprotonated anion. This formula matches indeed the $Al_2(OH)_6Hpgl^-$ complex, supporting the validity of the proposed model. Since Al^{3+} is a negligible species as compared to $Al(OH)_4^-$ in ligand-free solutions at this pH [25], the complex is likely to be formed *via* the binding of aluminates. That is, one $Al(OH)_4^-$ ion are coordinated by the COO^- and the adjacent OH group of the ligand, the other is bound by two other OH functionalities (for instance, the C3(OH) and C5(OH) ones). The binding is followed by three condensation steps between the OH moieties of $Hpgl^-$ and Al $(OH)_4^-$ releasing three water molecules. Simultaneously, one OH^- ion attached to each Al^{3+} ion is being protonated yielding H_2O. These two coordinated water molecules are likely to dissociate from the complex during the evaporation process. The possible structure of the complex is depicted in the inset of Fig. 5. Here we assume the geometry of the metal center to be tetrahedral.

3.3. Structural aspects of the complexation reactions and possible metal-binding sites

To gain structural insight of the complexes forming, we recorded a series of ^1H and ^{13}C NMR spectra as a function of pH and $[Al(OH)_4^-]_T$. Before any analysis concerning complexation, we have to note that for the pH-dependent ^1H and ^{13}C NMR (Figs. 6 and S8) as well as for the $[Al(OH)_4^-]_T$-dependent ^1H and ^{13}C NMR spectra at pH = 4 (Figs. S9 and S10), there are several peaks marked as 'L'. These signals are most likely to belong to the lactone form of heptagluconic acid. The formation of such ring compounds is common for hydroxycarboxylic acids, such as gluconic acid [26]. Due to its rigid structure, the lactones are in general do not participate in metal complexation; hence, we focus solely on the ligand peaks in the following discussion.

For the solution with $[Al(OH)_4^-]_T = [Hpgl^-]_T = 0.200$ M and at pH = 4, the dominant species is the $Al_2(OH)_4Hpgl_2^0$ dimer; see the speciation diagram of heptagluconate in Fig. 7. The ^1H spectrum (Fig. 6) shows that the chemical exchange between and the free and complexed ligand is rather slow, giving rise to broad and thus not well-resolved signals. This is in line with the $[Al(OH)_4^-]_T$-dependent spectra at the same pH (Fig. S9); that is, the signal half-widths increase

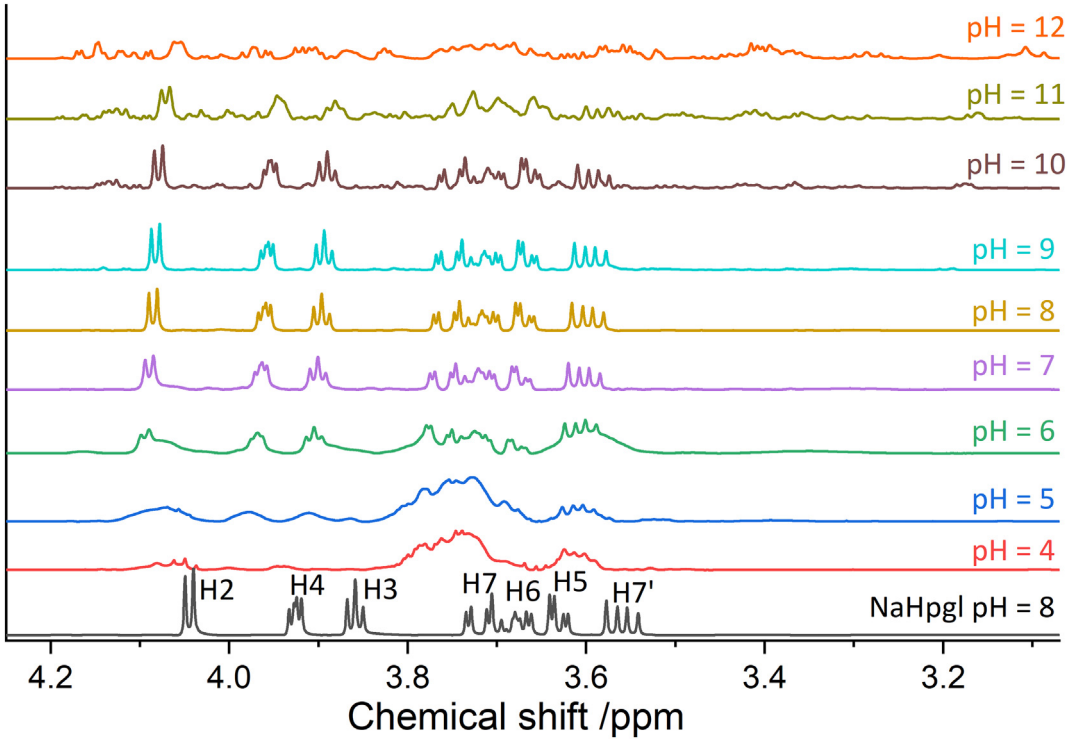

Fig. 6. ^{1}H NMR spectra of solutions containing $[Al(OH)_4^-]_T = [Hpgl^-]_T = 0.200$ M as a function of the nominal pH at (25 ± 1) °C.

gradually, particularly the C2H(OH), C3H(OH) and the C4H(OH) ones. This indicates their vital roles as coordination sites. The drop in the relative intensity of the C1–C5 in the ^{13}C spectra confirms this observation (Fig. S10), and suggests the participation of the COO^- and C5(OH) groups in the metal ion-binding. Furthermore, the slow exchange is indicative of strong metal-ligand interactions. We can elucidate this feature by the high charge density of the metal, resulting in strong coordinative bonds between Al^{3+} and the COO^- as well as the OH groups. In turn, the coordination of Al^{3+} leads to the weakening of the O—H bonds. In turn, the acidity of the OH function decreases, that is, the deprotonation of the OH group can occur at much lower pH than in the metal-free system ((pK = 13.8, Table 1). This the well-known metal-ion-induced ligand deprotonation and its driving force is the formation of stable chelate rings with the Al^{3+} ion being bound to the COO^- and (at least) one alcoholate moiety.

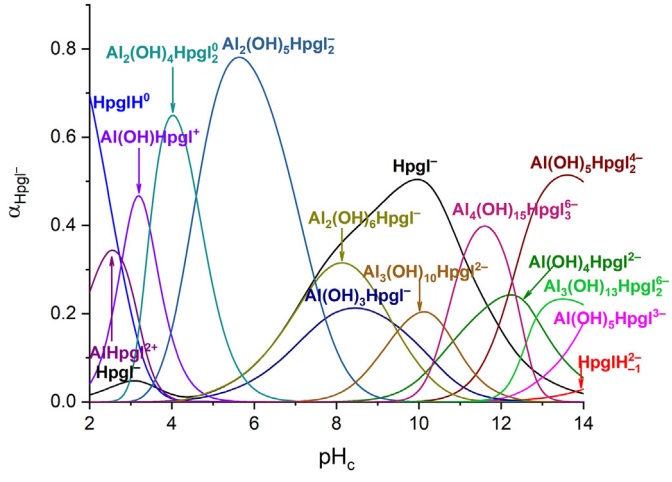

Fig. 7. Speciation diagram as a function of pH_c in regard to $Hpgl^-$. The calculations were on the basis of stability constants provided in *Table* 1, corresponding to T = (25 ± 0.1)°C and I = 4 M (NaCl). Total concentrations: $[Al(OH)_4^-]_T = 0.200$ M and $[Hpgl^-]_T = 0.200$ M.

This is further supported by the fact that the first deprotonation step referring to the reaction:

$$AlHpgl^{2+} \rightleftharpoons AlHpglH_{-1}^{+} + H^+ \quad (9)$$

has a pK of 3.6 ($\log \beta_{114} - \log \beta_{113}$, Table 1), being much lower than that of the Al^{3+} aqua-ion (pK = 5.5 at I = 3 M NaCl [24]). This indicates that the first deprotonation step indeed occurs on the ligand rather than on a metal-coordinated water molecule, similarly to the Al(III)/$Gluc^-$ system [12]. Whether the second deprotonation takes place on the ligand or on a water molecule yielding the putative $Al(OH)_2Hpgl^0$ species (and its dimer), however, is not deductible from the NMR spectra.

Increasing the pH further up to 9, we observe the recovery of the spectrum of the plain ligand (Figs. 6 and S8). This becomes obvious when we compare the spectrum at pH = 8 with the one of $Hpgl^-$ at the same pH (Fig. 6). Moreover, increasing $[Al(OH)_4^-]_T$ at pH = 8 results in only a minor downfield shift of the ^{1}H peaks (Fig. S11) and no noticeable variations in the ^{13}C spectra (Fig. S12). Consequently, the complexes formed in the pH range of 6–9 are in fast exchange with the free ligand. The acceleration of the chemical exchange upon the pH increase implies the weakening of metal-ligand interactions. A possible (however speculative) explanation for this striking feature is that further deprotonation takes place on coordinated water molecules. The strong bond between Al^{3+} and OH^- ions leads to the apparent destabilization of those between Al^{3+} and $Hpgl^-$. This scenario seems to be valid for all species formed in this range, particularly for $Al_2(OH)_6Hpgl^-$ being the predominant one (Fig. 7). Furthermore, n_{OH}: $n_{Al} \geq 3$ holds for all complex compositions, suggesting the formation of $Al(OH)_3$ moieties being loosely bound to the ligand through the COO^- group.

Concerning $Al_2(OH)_6Hpgl^-$, this finding is in contradiction with the structure sketched in Fig. 5, where strong Al–O–C bonds are present. As an attempt to resolve this contradiction, we propose this species to be in the form of $Al_2(OH)_6Hpgl^-$ in solution with Al^{3+} being sixfold coordinated. A possible isomerization of the metal center from octa- to tetrahedral geometry during the MS measurement facilitates the condensation reactions to take place, resulting in the formation of the $Al_2(OH)_2HpglH_{-3}^-$ complex (Fig. 5). Interestingly, such change in the

coordination number was suggested for the $Al(OH)_3Gluc^-$ complex previously [10].

Both the ^1H and ^{13}C spectra above pH = 10 (Figs. 6 and S8) exhibit again salient variations, namely, the appearance of new peaks which correspond to newly-formed complexes. This is apparent in the $[Al(OH)_4^-]_T$-dependent ^1H and ^{13}C spectra at pH = 12 (Figs. S13 and S14). The emergence of distinct peaks of the complexes indicates that the ligand exchange rate is even slower than that at pH = 4. The slow-down of the exchange processes signals the formation of species that are considered to be inert on the NMR timescale and again reflects strong metal-ligand interactions. This must be the consequence of Al–O–C ethereal-type bonds of highly covalent nature, forming *via* intermolecular condensation reactions. (This mechanism and the concomitant slow exchange is known for the Al(III)/$Gluc^-$ system [13].) On the other hand, the deprotonation of the ligand results in similar Al–O–C bonds being present already at pH = 4 (Figs. 6 and S8). Why in that case the exchange rate is somewhat faster, might be answered by the different geometry. That is, the dissociation of the complexes is slower when coordination geometry of the metal center is octahedral when it is tetrahedral. This leads to the interesting presumption that the change in the coordination geometry occurs in the neutral to mildly alkaline pH regime.

Furthermore, the ^{13}C spectrum at pH = 12 (Fig. 8) exhibits eight additional peaks around the C1 as well as the C7 peaks of the free ligand (being present at ≈20%, see Fig. 7). In addition to $Hpgl^-$, three complexes dominate the equilibria, namely $Al(OH)_4Hpgl^{2-}$, $Al(OH)_5Hpgl_2^{4-}$ and $Al_4(OH)_{15}Hpgl_3^{6-}$. The presence of eight complex signals clearly shows that these species exist in isomeric forms. It is also important to note that a further deprotonation occurs on $Al(OH)_4Hpgl^{2-}$ yielding $Al(OH)_5Hpgl^{3-}$ (and $Al(OH)_5Hpgl_2^{4-}$). The existence of a five-coordinated Al^{3+} in strongly alkaline medium is a long-running conundrum in the inorganic chemistry society [27]. Whether this is the case in the present system cannot be concluded from our experiments. We believe that future extended X-ray absorption fine structure (EXAFS) measurements could help to clarify this question.

4. Conclusion

The complex formation between $Al(OH)_4^-$ and $Hpgl^-$ ions was studied in acidic to highly alkaline solutions at 25°Cand 4 M ionic strength. Potentiometric titrations revealed the formation of several mono– and polynuclear complexes in the alkaline region, greatly extending the speciation models published earlier in the literature. It was found, that the mononuclear 1:1 complex undergoes a gradual protonation, while the species $Al(OH)_2Hpgl^-$ coordinates to additional two aluminate ions, forming 2:1 and even 3:1 stoichiometry particles.

Polarimetric measurements further broadened the speciation, by the inclusion of $Al_3(OH)_{13}Hpgl_2^{6-}$ and $Al_4(OH)_{15}Hpgl_3^{6-}$ species, while corroborated the model obtained previously by potentiometry.

^1H and ^{13}C NMR measurements provided qualitative insight on the binding sites of the ligand measured at pH = 4. Based on the spectra obtained at neutral pH, the forming species are ligand–stabilized hydroxides. This assumption was strengthened by semi-quantitative solubility simulations, which showed, that in the pH range from 6 to 11 the total concentration of Al^{3+} and OH^- exceeded the solubility product of $Al(OH)_3$, yet no precipitation could be observed in these solutions in the presence of heptagluconate ions. The earlier studies published for the related D-gluconate showed, that in the presence of the ligand, the active growth surface during crystallization is blocked, greatly delaying or even stopping the process. In strongly alkaline media, complexation proved to be a slow process, thus being commensurate with the exchange rate of free and bind ligand, yielding numerous new peaks on the spectra. According to the obtained speciation diagram, these new peaks can belong both to the coordination isomers of $Al(OH)_4Hpgl^{2-}$ or the polynuclear $Al_4(OH)_{15}Hpgl_3^{6-}$ complexes.

The results in the present work were verified by freezing point depression and ESI–MS studies, too. FPD measurements indicated a large extent of association in solutions containing both aluminate and heptagluconate, while in the individual solutions, this effect was not detectable. The simulated $\Delta T_{f,calc}$ values, based on the calculated speciation data, were in good agreement with the measured changes. (For more details, see Section 2 and Table S2 in the ESI.) ESI–MS measurements supported the results by detecting the dominant 2:1 species at pH = 7, and provided indirect information about the coordination mode in the complex as well.

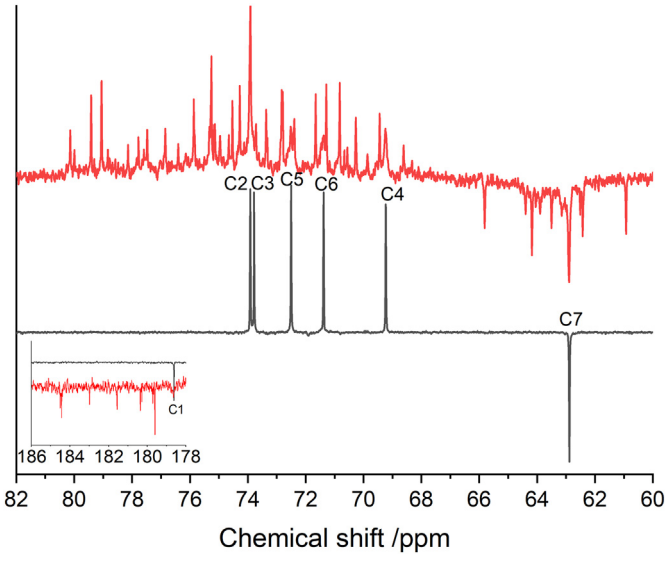

Fig. 8. Comparison of ^{13}C NMR spectra of a solution containing only $[Hpgl^-]_T = 0.200$ M (black spectrum) with one containing $[Hpgl^-]_T = 0.200$ and $[Al(OH)_4^-]_T = 0.200$ (red spectra) at pH = 12 and 25 °C ± 1 °C. (For interpretation of the references to colour in this figure legend, the reader is referred to the web version of this article.)

CRediT authorship contribution statement

Ákos Buckó: Data curation, Formal analysis, Investigation, Methodology, Validation, Visualization, Writing - original draft.**Bence Kutus:**Conceptualization, Formal analysis, Investigation, Resources, Software, Supervision, Validation, Visualization, Writing - review & editing.**Gábor Peintler:**Data curation, Formal analysis, Software.**Zoltán Kele:**Investigation, Validation.**István Pálinkó:**Conceptualization, Funding acquisition, Project administration, Resources, Supervision, Writing - review & editing.**Pál Sipos:**Conceptualization, Funding acquisition, Project administration, Resources, Supervision, Writing - review & editing.

Declaration of competing interest

The authors declare that they have no known competing financial interests or personal relationships that could have appeared to influence the work reported in this paper.

Acknowledgment

This research was funded by the NKFIH K 124265 Grant, which is highly appreciated. Insightful comments from Prof. Tamás Kiss are gratefully acknowledged.

Appendix A. Supplementary data

Supplementary data to this article can be found online at https://doi.org/10.1016/j.molliq.2020.113645.

References

[1] N. Greenwood, A. Earnshaw, Chemistry of the Elements, 2nd edition Butterworth-Heinemann, Oxford, UK, 1997.
[2] D. Donaldson, B.E. Raahauge (Eds.), Essential Readings in Light Metals, Volume 1: Alumina and Bauxite, John Wiley & Sons, Hoboken, NJ, U.S., 2013
[3] G. Power, J. Loh, Organic compounds in the processing of lateritic bauxites to alumina, Hydromet 105 (2010) 1–29.
[4] G. Power, J.S. Loh, C. Vernon, Organic compounds in the processing of lateritic bauxites to alumina. Part 2: effects of organics in the Bayer process, Hydromet 127–128 (2012) 125–149.
[5] B.I. Whittington, The chemistry of CaO and $Ca(OH)_2$ relating to the Bayer process, Hydromet 43 (1996) 13–35.
[6] F.R. Venema, J.A. Peters, H. van Bekkum, Multinuclear-magnetic-resonance study of the coordination of aluminium (III)-aldarate complexes with calcium(II) in aqueous solution, Recl. Trav. Chim. Pays-Bas 112 (1993) (1993) 445–450.
[7] A. Pallagi, É.G. Bajnóczi, S.E. Canton, T. Bolin, G. Peintler, B. Kutus, Z. Kele, I. Pálinkó, P. Sipos, Multinuclear complex formation between Ca(II) and gluconate ions in hyperalkaline solutions, Environ. Sci. Technol. 48 (2014) 6604–6611.
[8] Á. Buckó, B. Kutus, G. Peintler, I. Pálinkó, P. Sipos, Temperature dependence of the acid–base and Ca^{2+}-complexation equilibria of D-gluconate in hyperalkaline aqueous solutions, Polyhedron 158 (2019) 117–124.
[9] R.J. Motekaitis, A.E. Martell, Complexes of aluminum(III) with hydroxy carboxylic acids, Inorg. Chem. 23 (1984) 18–23.
[10] W.M. Best, M.H. Jack, M.S. Todd, W.S. Robert, Aluminum(III) coordination to hydroxy carboxylates: the influence of hydroxy substituents enabling tridentate binding, Aust. J. Chem. 47 (1994) 2023–2031.
[11] G.M. Escandar, A.C. Olivieri, M. González-Sierra, A.A. Frutos, L.F. Sala, Complexation of aluminium(III), gallium(III) and indium(III) ions with D-gluconic and lactobionic acids. A potentiometric and nuclear magnetic resonance spectroscopic study, J. Chem. Soc. Dalton Trans. (1995) 799–804.
[12] A. Lakatos, T. Kiss, R. Bertani, A. Venzo, V.B. Di Marco, Complexes of Al(III) with d-gluconic acid, Polyhedron 27 (2008) 118–124.
[13] A. Pallagi, Á.G. Tasi, G. Peintler, P. Forgó, I. Pálinkó, P. Sipos, Complexation of Al(III) with gluconate in alkaline to hyperalkaline solutions: formation, stability and structure, Dalton Trans. 42 (2013) 13470–13476.
[14] P. Sipos, P.M. May, G.T. Hefter, Carbonate removal from concentrated hydroxide solutions, Analyst 125 (2000) 955–958.
[15] P. Sipos, S.G. Capewell, P.M. May, G. Hefter, G. Laurenczy, F. Lukács, R. Roulet, Spectroscopic studies of the chemical speciation in concentrated alkaline aluminate solutions, J. Chem. Soc. Dalton Trans. (1998) 3007–3012.
[16] I. Kron, S.L. Marshall, P.M. May, G. Hefter, E. Königsberger, The ionic product of water in highly concentrated aqueous electrolyte solutions, Monatsh. Chem. 126 (1995) 819–837.
[17] G. Peintler, B. Kormányos, B. Gyurcsik, pHCali, Version 1.32a, University of Szeged, Szeged, Hungary, 2007.
[18] A. Pallagi, Z. Csendes, B. Kutus, E. Czeglédi, G. Peintler, P. Forgo, I. Pálinkó, P. Sipos, Multinuclear complex formation in aqueous solutions of Ca(II) and heptagluconate ions, Dalton Trans. 42 (2013) 8460–8467.
[19] Waters Corp, MassLynx v4.2, Milford MA, US, 2019.
[20] L. Zékány, I. Nagypál, G. Peintler, PSEQUAD for Chemical Equilibria, Update 5.20, University of Debrecen, Debrecen and University of Szeged, Szeged, Hungary, 2018.
[21] I. Puigdomenech, Make Equilibrium Diagrams Using Sophisticated Algorithms (MEDUSA), Version 1, Royal Institute of Chemistry, Stockholm, Sweden, 2015.
[22] G.M. Escandar, L.F. Sala, Complexes of cu(II) with D-aldonic and D-alduronic acids in aqueous solution, Can. J. Chem. 70 (1992) 2053–2057.
[23] B. Kutus, C. Dudás, E. Orbán, A. Lupan, A.A.A. Attia, I. Pálinkó, P. Sipos, G. Peintler, Magnesium(II) d-gluconate complexes relevant to radioactive waste disposals: metal-ion-induced ligand deprotonation or ligand-promoted metal-ion hydrolysis? Inorg. Chem. 58 (2019) 6832–6844.
[24] C. Ekberg, P.L. Brown, Hydrolysis of Metal Ions, Wiley-VCH, Weinheim, Germany, 2016.
[25] C.F.J. Baes, R.E. Mesmer, The Hydrolysis of Cations, John Wiley & Sons, New York, NY, US, 1976.
[26] Z. Zhang, P. Gibson, S.B. Clark, G. Tian, P.L. Zanonato, L. Rao, Lactonization and protonation of gluconic acid: a thermodynamic and kinetic study by potentiometry, NMR and ESI-MS, J. Solut. Chem. 36 (2007) 1187–1200.
[27] P. Sipos, The structure of Al(III) in strongly alkaline aluminate solutions – a review, J. Mol. Liq. 146 (2009) 1–14.

Please cite this article as: Á. Buckó, B. Kutus, G. Peintler, et al., Stability and structural aspects of complexes forming between aluminum(III) and D-heptagluconate in ..., Journal of Molecular Liquids, https://doi.org/10.1016/j.molliq.2020.113645